Article

Cell Reports

OPA1 Isoforms in the Hierarchical Organization of Mitochondrial Functions

Graphical Abstract

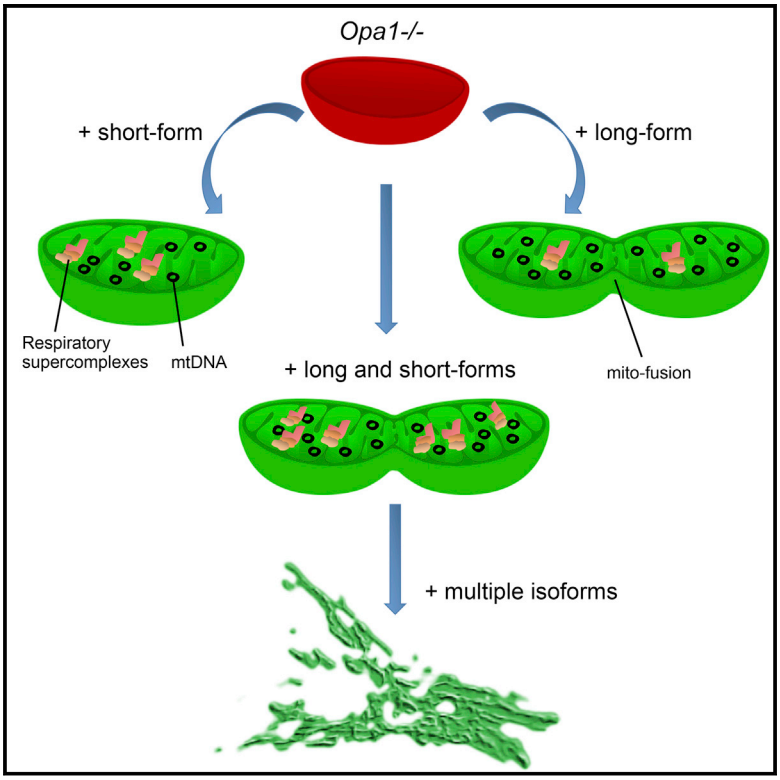

Highlights

- Any OPA1 isoform rescues mtDNA content, *cristae* organization, and energetics
- OPA1 long forms support mitochondrial fusion
- OPA1 short forms are better able to restore energetic efficiency
- Multiple OPA1 isoforms are required for mitochondrial dynamics

Authors

Valentina Del Dotto, Prashant Mishra, Sara Vidoni, ..., Michela Rugolo, Valerio Carelli, Claudia Zanna

Correspondence

michela.rugolo@unibo.it (M.R.), valerio.carelli@unibo.it (V.C.), claudia.zanna76@gmail.com (C.Z.)

In Brief

Del Dotto et al. perform a systematic analysis of the function of each of the eight OPA1 isoforms. They find that any OPA1 isoform can rescue mtDNA content, *cristae* structure, and mitochondrial energetics. A specific combination of long and short forms is required for mitochondrial dynamics and network morphology.

Del Dotto et al., 2017, Cell Reports *19*, 2557–2571
June 20, 2017
http://dx.doi.org/10.1016/j.celrep.2017.05.073

CellPress

Cell Reports
Article

OPA1 Isoforms in the Hierarchical Organization of Mitochondrial Functions

Valentina Del Dotto,[1,2,3] Prashant Mishra,[2] Sara Vidoni,[4] Mario Fogazza,[1] Alessandra Maresca,[5] Leonardo Caporali,[5] J. Michael McCaffery,[6] Martina Cappelletti,[1] Enrico Baruffini,[7] Guy Lenaers,[8] David Chan,[2] Michela Rugolo,[1,*] Valerio Carelli,[3,5,*] and Claudia Zanna[1,9,*]

[1]Department of Pharmacy and Biotechnology (FABIT), University of Bologna, 40126 Bologna, Italy
[2]Division of Biology and Biological Engineering, California Institute of Technology, Pasadena, CA 91125, USA
[3]Unit of Neurology, Department of Biomedical and NeuroMotor Sciences (DIBINEM), University of Bologna, 40139 Bologna, Italy
[4]Medical Research Council, Mitochondrial Biology Unit, Wellcome Trust, MRC Building, Cambridge CB2 0XY, UK
[5]IRCCS Institute of Neurological Sciences of Bologna, Bellaria Hospital, 40139 Bologna, Italy
[6]Integrated Imaging Center, Department of Biology, Johns Hopkins University, Baltimore, MD 21218, USA
[7]Department of Chemical Science, Life and Environmental Sustainability, University of Parma, 43124 Parma, Italy
[8]PREMMi, CNRS UMR6214, INSERM U1083, Université d'Angers, 49933 Angers Cedex 9, France
[9]Lead Contact
*Correspondence: michela.rugolo@unibo.it (M.R.), valerio.carelli@unibo.it (V.C.), claudia.zanna76@gmail.com (C.Z.)
http://dx.doi.org/10.1016/j.celrep.2017.05.073

SUMMARY

OPA1 is a GTPase that controls mitochondrial fusion, *cristae* integrity, and mtDNA maintenance. In humans, eight isoforms are expressed as combinations of long and short forms, but it is unclear whether OPA1 functions are associated with specific isoforms and/or domains. To address this, we expressed each of the eight isoforms or different constructs of isoform 1 in *Opa1*$^{-/-}$ MEFs. We observed that any isoform could restore *cristae* structure, mtDNA abundance, and energetic efficiency independently of mitochondrial network morphology. Long forms supported mitochondrial fusion; short forms were better able to restore energetic efficiency. The complete rescue of mitochondrial network morphology required a balance of long and short forms of at least two isoforms, as shown by combinatorial isoform silencing and co-expression experiments. Thus, multiple OPA1 isoforms are required for mitochondrial dynamics, while any single isoform can support all other functions. These findings will be useful in designing gene therapies for patients with OPA1 haploinsufficiency.

INTRODUCTION

OPA1 is a dynamin-related GTPase with a mitochondrial targeting sequence (MTS), which directs the protein to the inter-membrane space (IMS) and *cristae* volume (Olichon et al., 2002). OPA1 structure includes a transmembrane domain (TM), followed by coiled-coil domains, then the three highly conserved dynamin constituents: a GTPase domain, a middle domain, and a coiled-coil GTPase effector domain (GED). Eight OPA1 variants are present in humans, resulting from the alternative splicing of exons 4, 4b, and 5b with tissue-specific patterns of expression (Olichon et al., 2007a). The cleavage of the MTS produces the long isoforms (l-forms) anchored to the inner mitochondrial membrane (IMM). About half of l-forms are then constitutively processed by OMA1 and YME1L proteases in the domains corresponding to exons 5 and 5b, containing the cleavage sites S1 and S2, respectively, to generate the short isoforms (s-forms) devoid of the TM segment (MacVicar and Langer, 2016). Noticeably, l-forms including exon 4b are completely processed into s-forms (Song et al., 2007).

Many evidences associate OPA1 with crucial mitochondrial functions, including fusion of the IMM, shaping the *cristae* morphology, oxidative phosphorylation (OXPHOS) efficiency, and mtDNA maintenance (Belenguer and Pellegrini, 2013; Vidoni et al., 2013). OPA1 oligomerization, tightening *cristae junctions*, also controls the propensity to apoptosis by sequestering cytochrome *c* within the *cristae* and regulating its release in the IMS (Olichon et al., 2003; Frezza et al., 2006).

Global loss of OPA1 causes fragmentation of the mitochondrial network, associated with severe disorganization of *cristae* structure (Olichon et al., 2003; Song et al., 2007, 2009), as well as reduced cell proliferation, mitochondrial membrane potential, and respiratory capacity (Olichon et al., 2003; Cogliati et al., 2013) and depletion of mtDNA (Chen et al., 2010). Re-expression of OPA1 ameliorates *cristae* organization and mitochondrial network morphology (Cogliati et al., 2013; Patten et al., 2014). Interestingly, OPA1 overexpression also induces mitochondrial network fragmentation, suggesting that its amount is key to correctly maintaining mitochondrial network and *cristae* morphology (Cipolat et al., 2004; Olichon et al., 2007b). Alternatively, mild OPA1 overexpression promotes the stabilization of mitochondrial *cristae*, in turn leading to increased respiratory efficiency, allowing it to complement deleterious phenotypes found in mouse genetic models of mitochondrial diseases (Varanita et al., 2015). A combination of l- and s-forms is also necessary for efficient mitochondrial fusion (Song et al., 2007; DeVay et al., 2009), and proteolytic cleavage of l-forms stimulates

membrane fusion, integrating the sensing of energy requirements (Mishra et al., 2014). Others suggested that l-forms alone are sufficient for mitochondrial fusion and *cristae* organization (Ishihara et al., 2006; Anand et al., 2014).

OPA1 mutations are associated with dominant optic atrophy (DOA), one of the commonest inherited optic neuropathies, which is characterized by degeneration of the retinal ganglion cells and leads to optic nerve atrophy and ultimately to blindness (Alexander et al., 2000; Delettre et al., 2000; Lenaers et al., 2012). Pathophysiological studies, mainly performed on DOA patient fibroblasts, revealed that a variety of mitochondrial dysfunctions occur in *OPA1*-mutated cells, including disorganization of *cristae* structure, OXPHOS deficiency, altered mitochondrial network dynamics, and disturbed mtDNA maintenance (Belenguer and Pellegrini, 2013).

Although OPA1 functions have been studied for 15 years, it remains unclear whether they are associated with defined protein domains or are rather specifically linked to one or more isoforms. To tackle this issue, we used two experimental approaches: we expressed specific constructs of OPA1 isoform 1 (ISO1), which are modified at the N terminus, unable to generate the s-form, or with a defective GTPase domain, in mouse embryonic fibroblasts (MEFs) deleted for *Opa1* (*Opa1*$^{-/-}$ MEFs). We then expressed separately each isoform in *Opa1*$^{-/-}$ MEFs, as well as transiently expressed or silenced combinations of them. As mitochondrial function readouts, we considered *cristae* structure and mtDNA content, cell proliferation under metabolic stress, cell respiration and ATP synthesis rates, OXPHOS supercomplex assembly, mitochondrial fusion, and network morphology.

RESULTS

Expression of ISO1-Modified Constructs Elucidates the Role of OPA1 Domains in Rescuing the Defective Phenotypes of *Opa1*$^{-/-}$ MEFs

The lack of *Opa1* in MEFs caused complete fragmentation of the mitochondrial network, significant reduction of mtDNA copy number, and drastic disorganization of *cristae* structure (Song et al., 2007, 2009; Chen et al., 2010). Furthermore, *Opa1*$^{-/-}$ MEFs grew much slower than wild-type (WT) MEFs in DMEM-glucose, and they exhibited a drastic reduction in the oxygen consumption rate (OCR). The defective *Opa1*$^{-/-}$ MEF phenotype was substantially recovered for all mitochondrial functions by the expression of ISO1 (Patten et al., 2014), which is the most highly expressed in human tissues (Olichon et al., 2007a).

To assess whether different functions might be attributed to OPA1 domains common to all isoforms, we generated cell lines stably expressing WT and modified human ISO1 constructs (Figure S1A). To investigate the role of OPA1 l-forms in the absence of the s-form and the role of the GTPase domain, we used the ISO1 Long construct (ISO1 Long) (Song et al., 2007) and the ISO1 construct with the G300E DOA mutation in the GTPase domain (G300E) (Ban et al., 2010), respectively. Finally, a third construct was generated by replacing the N-terminal domain of ISO1 with the N-terminal domain of AIF, another IMS protein anchored to the IMM (Ishihara et al., 2006). This last construct (AIF-230) was designed to study the effect of the C-terminal portion of a l-form in the absence of its own N-terminal domain.

Western blotting confirmed that ISO1 and G300E were correctly cleaved in l- and s-forms, whereas ISO1 Long and AIF-230 presented a single band, corresponding to the uncleaved form, as predicted for these proteins lacking the S1 and S2 cleavage sites (Figure S1B).

We first tested the ability of each construct to rescue mtDNA levels. We observed that ISO1 and ISO1 Long completely recovered the mtDNA copy number, whereas the AIF-230 and G300E induced only a slight, non-significant, increase in mtDNA amount compared to *Opa1*$^{-/-}$ cells (Figure 1A). Concordantly, similar data were obtained by the quantification of nucleoids (Figures 1B and S1C). These results suggest that mtDNA content depends on the integrity of both OPA1 N terminus and GTPase domain.

Our quantitative analysis showed that none of the OPA1-modified constructs recovered the mitochondrial network morphology, in comparison with ISO1; ISO1 Long and AIF-230 led to an almost completely fragmented network, whereas the G300E induced an entirely fragmented network (Figures 1C and S1D). It has been previously reported that the lack of OPA1 prevents mitochondrial fusion even in the presence of stimuli that inhibit fission, such as nutrient deprivation (Gomes et al., 2011). To reconsider this aspect, cells expressing the ISO1 construct variants were starved with Hank's balanced salt solution (HBSS). ISO1 and ISO1 Long cells increased the percentage of elongated and intermediate mitochondria, nevertheless, without reaching the values of WT MEFs. The rescue of mitochondrial network morphology with AIF-230 was slightly reduced, and G300E still exhibited a totally fragmented network (Figure S1E).

To directly quantify the mitochondrial fusion, we expressed a photoactivable mitochondrial matrix-target GFP (mt-PAGFP), and we measured its dilution rate over time after photoactivation (Zanna et al., 2008). We observed efficient mitochondrial fusion in ISO1 and ISO1 Long cells, without reaching the values of WT MEFs. AIF-230 and G300E mitochondria displayed a negligible fusion competence, close to *Opa1*$^{-/-}$ mitochondria (Figures 1D and 1E). Thus, a cleavable isoform (i.e., ISO1) is required to maintain an interconnected mitochondrial network, whereas an l-form alone (ISO1 Long) is able to sustain the mitochondrial fusion. The integrity of the GTPase domain is essential to recover both the mitochondrial morphology and fusion competence. In addition, the phenotypes obtained by expressing our constructs indicate that the maintenance of the mtDNA content is dependent on mitochondrial fusion, but not on network morphology.

Investigation of mitochondrial ultrastructure by electron microscopy revealed a large heterogeneity in mitochondrial *cristae* number (Figure S2A), which we quantified by scoring mitochondria into three categories (Figures 2A and 2B) as follows: more than four *cristae* (class I), between two and three *cristae* (class II), and one or no *cristae* (class III) per mitochondrion. Furthermore, we distinguished physiological mitochondria with dense matrix (class A) from swollen mitochondria with hypodense matrix (class B) (Figures 2C and 2D). *Opa1*$^{-/-}$ cells exhibited severely abnormal ultrastructure, including swollen mitochondria and reduced *cristae* number. Conversely, in WT MEFs more than 70% of mitochondria belonged to class I and 100% to class A (Figures 2B and 2D). The *cristae* structure of

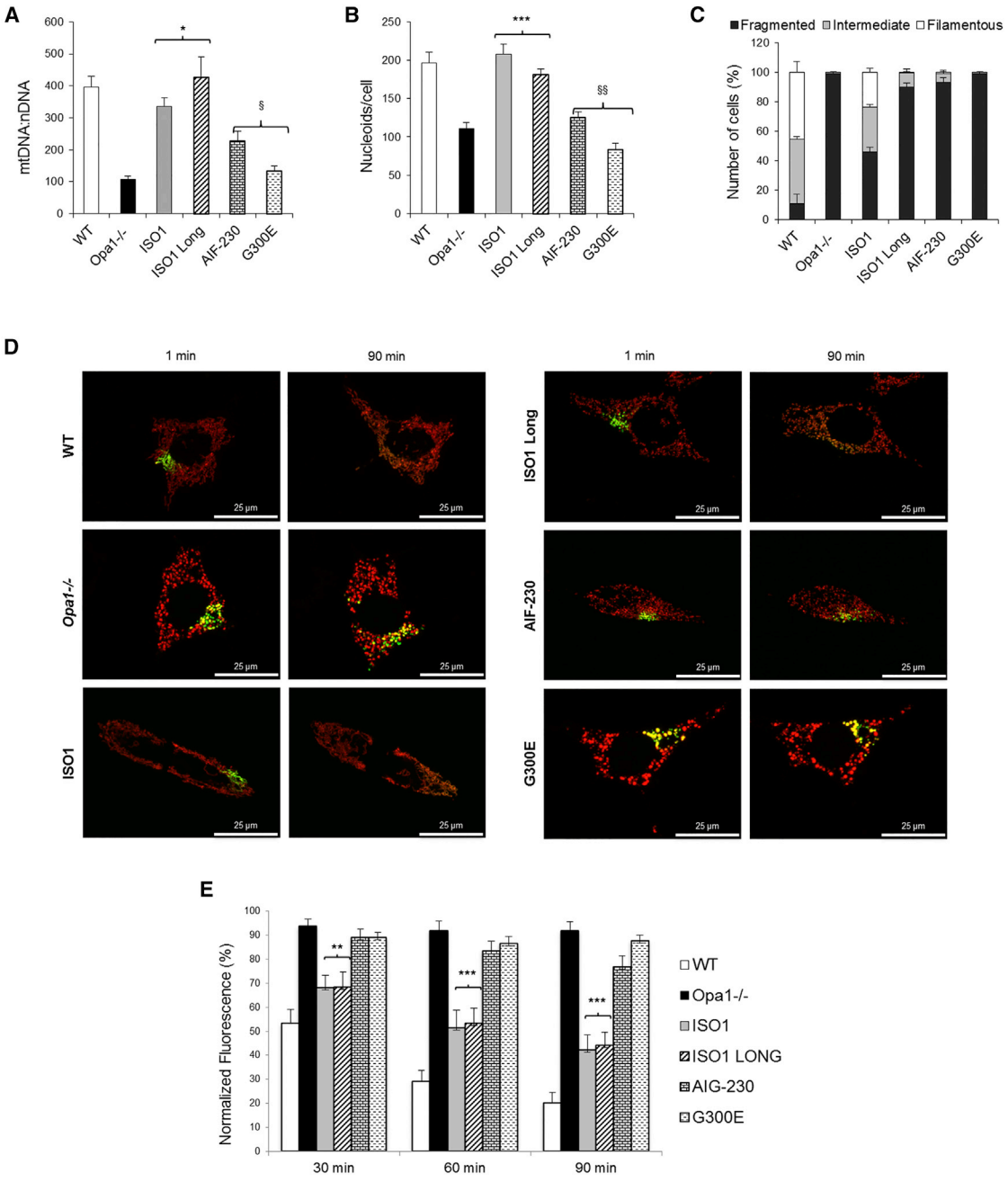

Figure 1. mtDNA Content, Mitochondrial Network Morphology, and Fusion of MEFs Expressing Different OPA1 Variants

(A) mtDNA copy number. Data are means ± SEM of at least three independent experiments (*values significantly different from the *Opa1*$^{-/-}$ MEF, $p < 0.05$; §values significantly different from WT MEF, $p < 0.05$).

(B) Number of nucleoids per cell. Data are means ± SEM (n = 30; ***values significantly different from the *Opa1*$^{-/-}$ MEF, $p < 0.001$; §§values significantly different from WT MEF, $p < 0.001$).

(C) Quantification of mitochondrial network immuno-labeled with TOM20 antibody of three independent experiments (means ± SEM, n = 100).

(D) The different cell lines were transfected with both mt-PAGFP (green) and mt-RFP (red), and mitochondrial fusion was monitored by the time-dependent dilution of mt-PAGFP fluorescence. Representative merged images at 1 and 90 min are shown.

(E) Quantification of mitochondrial fusion. The values of mt-PAGFP fluorescence after 30, 60, and 90 min were expressed as percentages of the fluorescence value at 1 min (100% value). Data are means ± SEM (n = 20; **and ***values significantly different from the *Opa1*$^{-/-}$ MEF, $p < 0.01$ and $p < 0.001$, respectively).

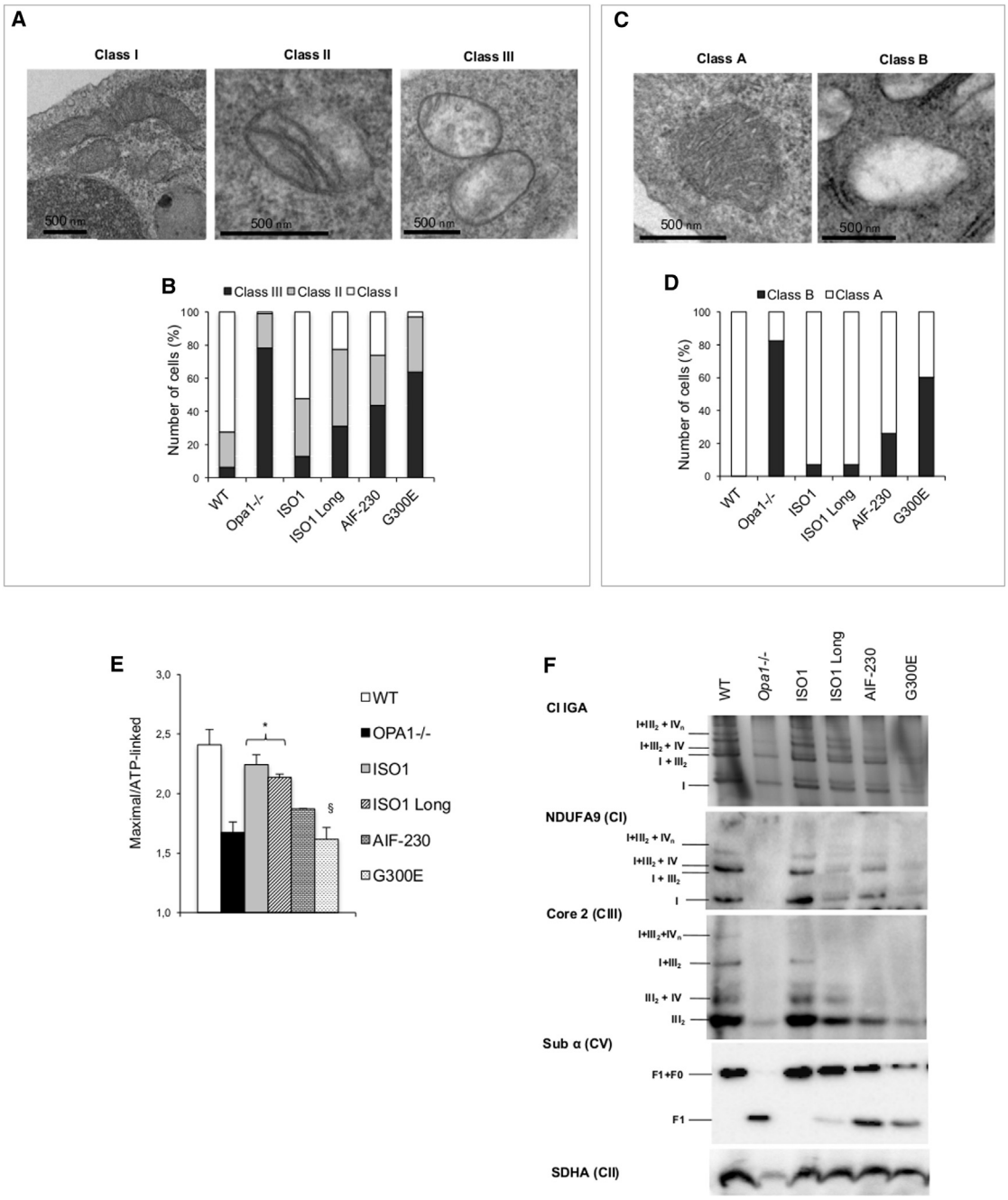

Figure 2. Mitochondrial *cristae* Morphology and Energetics Profile of MEFs Expressing Different OPA1 Variants

(A) Representative electron microscopy (EM) images of mitochondrial *cristae* number in MEFs.

(B) 40–60 mitochondria per sample were scored in three categories: more than four *cristae* (class I), between two and three *cristae* (class II), and one or no *cristae* (class III) per mitochondrion.

(C) Representative EM images of mitochondrial matrix density and swelling of MEFs.

(D) 40–60 mitochondria per sample were scored according to matrix density and swelling: dense matrix (class A) and swollen mitochondria with hypodense matrix (class B).

(E) Ratio between maximal and ATP-linked respiration. Data are means ± SEM of at least two determinations (*values significantly different from the *Opa1*$^{-/-}$ MEF, $p < 0.05$; §values significantly different from WT MEF, $p < 0.05$).

(F) Supercomplexes analyzed in digitonin-solubilized mitochondria by blue native (BN)-PAGE and evidenced by CI IGA and western blot. SDHA (CII) was used as a loading control. Supercomplex composition and single complexes are indicated. A representative experiment of three is shown.

G300E was similar to *Opa1*$^{-/-}$ MEFs, showing 60% class III and class B mitochondria. Expression of AIF-230 and ISO1 Long improved *cristae* organization with less class III mitochondria (40% and 30%, respectively), even if not comparable to ISO1, which displayed 50% class I mitochondria and 10% class III mitochondria (Figure 2B). Furthermore, this percentage of class B mitochondria was reduced to 25% in AIF-230 and almost absent in ISO1 and ISO1 Long cells (Figure 2D). Overall, these results reveal that the recovery of *cristae* morphology parallels the recovery of mtDNA abundance.

Cell growth in DMEM-glucose was significantly reduced only in G300E cells (Figure S2B). In DMEM-galactose, ISO1 Long cells grew slightly faster than ISO1 and WT MEFs, whereas AIF-230 cells grew slower, and G300E cells almost completely failed to proliferate (Figure S2C). Consistent with these results, mitochondrial respiration of G300E cells was similar to *Opa1*$^{-/-}$ MEFs (Figure S2D), whereas that of ISO1 Long and AIF-230 cells was improved, without reaching the levels of ISO1. The maximal/ATP-linked respiration ratio was also increased for all constructs compared to *Opa1*$^{-/-}$ MEFs, even if statistical significance was reached only with ISO1 Long (Figure 2E).

Finally, western blot analysis of supercomplexes in ISO1 Long, AIF-230, and G300E cells showed, respectively, an incremental loss of assembled I + III_2 and III_2 + IV supercomplexes compared to ISO1, the latter being similar to WT MEFs (Figure 2F). The high-molecular-weight bands corresponding to I + III_2 + IV and I + III_2 + IV_n supercomplexes were hardly detectable in ISO1 Long and not found in AIF-230 and G300E cells. The complex I in gel activity (IGA) exhibited a similar pattern. The amounts of isolated complex I and III were also lower in ISO1 Long compared to ISO1 or WT MEFs, and they were further decreased in AIF-230 and G300E cells. Furthermore, the assembly of monomeric complex V, totally disassembled in *Opa1*$^{-/-}$ MEFs, was almost completely recovered in ISO1 Long, but only partially rescued in AIF-230 and G300E. Noticeably, despite the differences in the *cristae* ultrastructure and OXPHOS function/assembly evidenced among the cell lines, no significant alteration in reactive oxygen species (ROS) production was detected (Figures S2E–S2G).

These results suggest that the presence of an uncleavable isoform (ISO1 Long) or an isoform lacking the original OPA1 N-terminal domain (AIF-230) prevents full recovery of the OXPHOS parameters and supercomplex assembly. Thus, the complete rescue of the energetic competence requires the expression of a cleavable OPA1 variant with an intact GTPase domain.

All OPA1 Isoforms Restore mtDNA Content and Mitochondrial Ultrastructure Independently of the Network Morphology

To dissect their specific role in mitochondrial functions, we stably expressed each of the eight human OPA1 isoforms at the same amount in *Opa1*$^{-/-}$ MEFs, without the confounder of different protein expression (Figure S3A).

The amount of exogenously expressed OPA1 isoforms (Figure S3B) was slightly higher than the endogenous one from WT MEFs (1.2- to 2.2-fold increase; Figure S3C), but not significantly different among the eight cell lines and without consequences on the levels of other proteins involved in mitochondrial fusion and fission (Figure S3D). The eight OPA1 isoforms underwent correct proteolytic cleavage, with isoforms 1, 2, 4, and 7 appearing as both l- and s-forms, whereas isoforms 3, 5, 6, and 8 fully processed to s-forms (Song et al., 2007).

Expression of each isoform significantly rescued mtDNA copy number and nucleoid content, suggesting that the presence of the OPA1 N terminus is essential for mtDNA maintenance even after OPA1 cleavage, as in cells expressing only the s-form (Figures 3A, 3B, and S3E).

Evaluation of mitochondrial morphology indicated that cells expressing only the s-forms (isoforms 3, 5, 6, and 8) failed to rescue the network morphology, leaving mitochondria completely fragmented. Conversely, the presence together of l- and s-forms (isoforms 1, 2, 4, and 7) significantly increased mitochondrial tubulation, which still remained lower than in WT MEFs (Figure 3C). Noticeably, after HBSS incubation, the percentage of intermediate mitochondria increased also in cells expressing the s-form only, clearly suggesting that, when fission is blocked, the s-forms can ameliorate mitochondrial network morphology. Again, the percentage of recovery of filamentous network obtained in *Opa1*$^{-/-}$ cells expressing the different isoforms was lower compared to WT MEFs (Figure S3F). The cells expressing isoforms generating both l- and s-forms presented a substantial mitochondrial fusion rate, only slightly reduced compared to WT MEFs, whereas the rate was lower in cells expressing s-forms only (Figures 3D and 3E).

Finally, representative images of mitochondrial ultrastructure (Figure 4A) revealed a marked increase in class I mitochondria for all the isoforms and a negligible percentage of class B mitochondria, supporting a substantial recovery of mitochondrial ultrastructure independent of the mitochondrial network morphology (Figures 4B and 4C).

Each OPA1 Isoform Is Competent to Drive the Mitochondrial Energetic Efficiency Independently of Network Morphology

Both in DMEM-glucose and DMEM-galactose, MEFs expressing each isoform were as effective as WT MEFs in growth capacity, without differences among the isoforms (Figures S4A and S4B). In addition, their expression robustly increased mitochondrial respiration (Figures S4C–S4F). In particular, the ratios between maximal and ATP-linked respiration were completely recovered (Figure 4D), as were the ATP synthesis rates (Figure 4E). The supra-molecular organization of respiratory complexes was recovered, as shown by the band intensities related to complex I and the I + III_2 supercomplex (Figure 4F). The higher molecular weight I + III_2 + IV supercomplex was also present, except for isoforms 2 and 7, although the complex I IGA was similar for all the isoforms and comparable to that of WT MEFs. The levels of complex III dimer and of III_2 + IV supercomplex as well as the complex V assembly were also restored. As observed previously in cells expressing the tree constructs, the different OPA1 isoforms did not increase ROS production (Figures S4G–S4I).

In summary, these results indicate that the expression of each of the eight isoforms restores the overall energetic competence of *Opa1*$^{-/-}$ MEFs to levels similar to WT MEFs, independently of the mitochondrial network morphology.

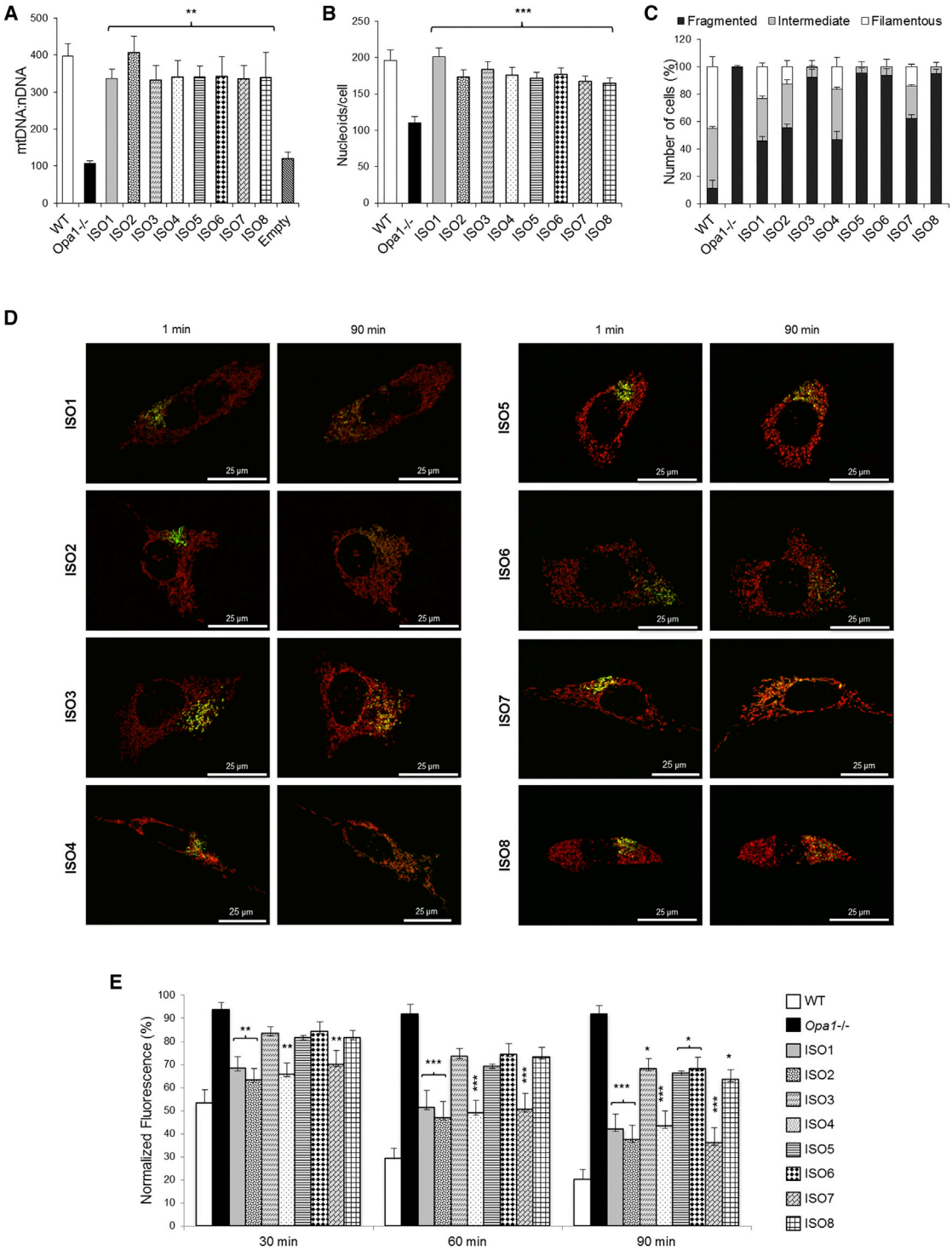

Figure 3. mtDNA Content, Network Morphology, and Fusion of MEFs Expressing the OPA1 Isoforms

(A) mtDNA copy number. Data are means ± SEM of at least three different experiments (**values significantly different from *Opa1*$^{-/-}$ MEFs, $p < 0.01$).

(B) Number of nucleoids per cell. Data are means ± SEM (n = 30; ***values significantly different from the *Opa1*$^{-/-}$ MEF, $p < 0.001$).

(C) Mitochondrial network was scored as in Figure 1C; error bars indicate SEM of three independent experiments.

(D) Representative merged images (mt-PAGFP in green and mt-RFP in red) of mitochondrial fusion at 1 and 90 min are shown.

(E) Quantification of mitochondrial fusion as in Figure 1E. Data are means ± SEM (n = 20; *$p < 0.05$, **$p < 0.01$, and ***$p < 0.001$).

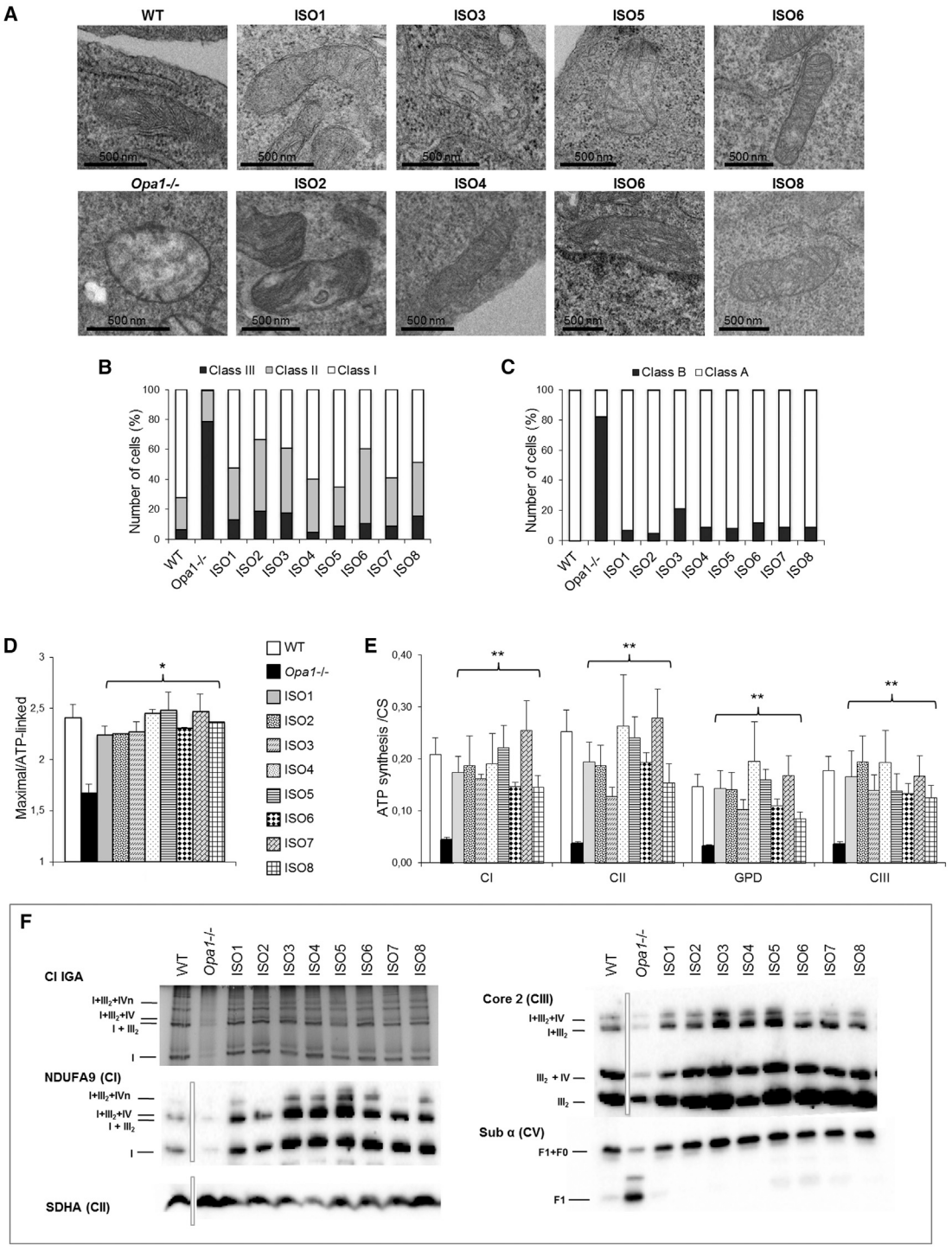

Figure 4. *cristae* Morphology and Energetics Profile of MEFs Expressing the OPA1 Isoforms

(A) Representative transmission electron microscopy (TEM) images of MEFs expressing the eight isoforms.

(B and C) Mitochondrial ultrastructure was scored according to *cristae* number (B) as in Figure 2B and to matrix density/swelling (C) as in Figure 2D. Approximately 40–60 mitochondria per sample were analyzed.

(D) Ratio between maximal and ATP-linked respiration. Data are means ± SEM of at least two determinations (*$p < 0.05$).

(E) ATP synthesis rates. Data are means ± SEM of at least three determinations (**$p < 0.01$).

(F) Supercomplexes analyzed by BN-PAGE and evidenced by CI IGA and western blot. SDHA (CII) was used as a loading control. Supercomplex composition and single complexes are indicated. A representative experiment of three is shown. Bars indicate that one lane was removed from the blot.

Multiple OPA1 Isoforms, At Least Two, Are Required to Fully Recover the Mitochondrial Network Morphology

The results described above indicate that there are no specific functions associated with each of the eight OPA1 isoforms, with the only exceptions being for the mitochondrial fusion and the network morphology that require the presence of both l- and s-forms, thus, isoform 1, 2, 4, or 7. Considering the partial rescue of mitochondrial network shape obtained with the expression of one of these isoforms, we transiently co-expressed a second OPA1 isoform, playing on different combinations (Table 1), to manipulate the mixture of how many short and long forms are theoretically generated. Expression of the second OPA1 isoform was confirmed by western blot analysis, and it revealed an increase of the l- or s-forms depending on the second isoform transfected (Figure 5A). OPA1 slight overexpression did not change the mitofusins' levels, but it was counterbalanced by increased DRP1 expression, equilibrating the fission/fusion machinery (Figure S5A). Being also the second isoform overexpressed, we could analyze the effects of the proportion of l- and s-forms without the interference of a different protein amount.

In ISO1 MEFs, the expression of ISO2 or ISO3 induced a complete rescue of mitochondrial network morphology, with the ISO2 being slightly more efficient than ISO3 (combination of 2long + 2short and 1long + 2short, respectively; Table 1) (Figures 5B and 5C). Conversely, in the same cells, the addition of ISO1 Long worsened the network morphology of ISO1 MEFs (2long + 1short) (Figures S5B and S5C). Starting from the totally fragmented network displayed by ISO1 Long, the addition of the ISO3 (1long + 1short) promoted an increase in filamentous and intermediate mitochondria more efficiently than adding ISO2 (2long + 1short) (Figures 5B and 5C). Conversely, starting from the totally fragmented network displayed by ISO3, the addition of ISO1 or ISO2 (1long + 2short) or of ISO1 Long (1long + 1short) was more efficient than adding only ISO5 (2short) (Figures 5B, 5C, S5B, and S5C). Finally, when the complete mitochondrial network fragmentation is due to a mutation in the GTPase domain (G300E), the insertion of ISO2 (2long + 2short) minimally rescued the network morphology, slightly better than adding ISO3 (1long + 2short) or ISO1 Long (2long + 1short) (Figures 5B, 5C, S5B, and S5C). The co-expression with the empty vector did not change the network morphology (Figures S5B and S5C). Overall, the presence of two OPA1 isoforms is required to fully restore network morphology, and an imbalance toward excessive l-forms or s-forms is counterproductive, maintaining the mitochondrial network fragmented (Table 1).

We then decided to further unwrap this issue by an opposite strategy, selectively depleting OPA1 isoforms in WT HeLa cells, using isolated or combined transfection of small interfering RNAs (siRNAs) targeting exons 4, 4b, and 5b, a control siRNA targeting all OPA1 variants (OPA1-kd), and a scramble siRNA.

OPA1 protein levels were markedly reduced by using the OPA1-kd, exon 4, exon 4 + 4b, and exon 4 + 5b siRNAs, and they were almost unchanged by exon 4b, 5b, and 4b + 5b silencing conditions (Figure 5D), in agreement with the respective abundances of each alternate exon in *OPA1* transcripts (Olichon et al., 2007a). As expected, the mitochondrial network morphology of control cells (untreated and scramble) was highly filamentous. Differently, cells transfected with OPA1-kd, exon 4, exon 4 + 4b, or exon 4 + 5b siRNA had a fragmented mitochondrial network (Figures 5E and 5F). In particular, exon 4 silencing led to expressing only the less abundant ISO2, 3, 4, and 6 (2long + 4short) (Table 1). The further silencing of exon 4b or 5b left in the cells ISO2 and 4 or ISO2 and 3, respectively, all barely expressed. Conversely, exon 4b- or exon 5b-silenced cells exhibited a filamentous mitochondrial network (Figures 5E and 5F). In exon 4b-silenced cells, the four isoforms left were ISO1, 2, 4, and 7, with ISO1 and ISO7 highly expressed, all generating l- and s-forms (4long + 4short). In exon 5b-silenced cells were left two isoforms generating l- and s-forms (ISO1 and 2) and two isoforms generating only s-forms (ISO3 and 5) (2long + 4short). In this latter condition, ISO1 was the only highly expressed. Finally, in exon 4b + 5b-silenced cells, the two isoforms left were ISO1 and 2, both leading to l- and s-forms (2long + 2short), with ISO1 again being the one highly expressed (Table 1).

In conclusion, in HeLa cells, the maintenance of a filamentous mitochondrial network is associated with the expression of a proper amount of OPA1 protein, in combination with a balanced mixture of OPA1 l- and s-forms or slightly unbalanced toward the s-forms. Excesses of l-form or s-form only are inefficient in maintaining a physiological morphology of the mitochondrial network.

DISCUSSION

Due to the molecular heterogeneity and complexity of OPA1 isoforms, we systematically tackled the unsolved issue of their roles in mitochondrial physiology. To this end, we adopted a set of molecular strategies assessing the implication of each isoform or combinations of them on clear-cut multiple readouts of OPA1 functions in cells with a genetic background totally devoid of OPA1.

The first result was that the expression of any of the eight isoforms was sufficient to maintain a physiological level of mtDNA content, build the *cristae*, and organize the structural and functional respirasome. The second result was that the proper amount and the multiplicity of OPA1 isoforms, respecting a specific combination between l- and s-forms, were required to fully recover mitochondrial network morphology. The sophisticated processing of l-forms to s-forms ensures a balanced organization of the mitochondrial network, having eight isoforms that provide a large degree of flexibility for a fine adaptive tuning to the cell needs.

Our results show that the s-form alone (i.e., ISO3) is minimally effective in recovering mitochondrial fusion, whereas the l-form alone (i.e., ISO1 Long) has a fusogenic competence comparable to l- and s-forms together (i.e., ISO1), even with a mitochondrial network almost completely fragmented. Thus, fusion capacity and mitochondrial morphology are not equivalent and need to be considered as distinct. The double knockout of OMA1 and YME1L proteases in MEFs or in cardiomyocytes demonstrated that the presence of l-forms only is sufficient to maintain mitochondrial fusion and also the network morphology (Anand et al., 2014; Wai et al., 2015). We should emphasize the different

Table 1. Combination of OPA1 Isoforms in MEFs and HeLa Cells

MEFs Stably Expressing One Isoform	Transient Expression of the Second Isoform	L-S Combination
ISO1 = 1long and 1short	ISO2 = 1long and 1short	2long + 2short
	ISO3 = 1short	1long + 2short
	ISO1L = 1long	2long + 1short
ISO1 Long = 1long	ISO2 = 1long and 1short	2long + 1short
	ISO3 = 1short	1long + 1short
ISO3 = 1short	ISO1 = 1long and 1short	1long + 2short
	ISO2 = 1long and 1short	1long + 2short
	ISO5 = 1short	2short
	ISO1L = 1long	1long + 1short
G300E = 1long and 1short	ISO2 = 1long and 1short	2long + 2short
	ISO3 = 1short	1long + 2short
	ISO1L = 1long	2long + 1short
siRNA HeLa Cells	**Isoforms Left after siRNA**	**L-S Combination**
NT or SCRAMBLE	ISO1 = 1long and 1short[a]	4long + 8short
	ISO2 = 1long and 1short	
	ISO3 = 1short	
	ISO4 = 1long and 1short	
	ISO5 = 1short[b]	
	ISO6 = 1short	
	ISO7 = 1long and 1short[a]	
	ISO8 = 1short[b]	
OPA1-kd	–	–
Ex4	ISO2 = 1long and 1short	2long + 4short
	ISO3 = 1short	
	ISO4 = 1long and 1short	
	ISO6 = 1short	
Ex4b	ISO1 = 1long and 1short[a]	4long + 4short
	ISO2 = 1long and 1short	
	ISO4 = 1long and 1short	
	ISO7 = 1long and 1short[a]	
Ex5b	ISO1 = 1long and 1short[a]	2long + 4short
	ISO2 = 1long and 1short	
	ISO3 = 1short	
	ISO5 = 1short[b]	
Ex4 + 4b	ISO2 = 1long and 1short	2long + 2short
	ISO4 = 1long and 1short	
Ex4 + 5b	ISO2 = 1long and 1short	1long + 2short
	ISO3 = 1short	
Ex4b + 5b	ISO1 = 1long and 1short[a]	2long + 2short
	ISO2 = 1long and 1short	

MEFs stably expressing the indicated isoform (first column) after transient expression with the indicated second one (second column) and the sum of the long and short forms present (third column). HeLa cells silenced with the indicated siRNAs (first column), isoforms left in the cell after silencing (second column), and the sum of the long and short forms present (third column).

[a]The OPA1 isoforms mostly expressed in HeLa cells.

[b]The OPA1 isoforms moderately expressed in HeLa cells; no footnote indicates the OPA1 isoforms were poorly expressed in HeLa cells (Olichon et al., 2007a).

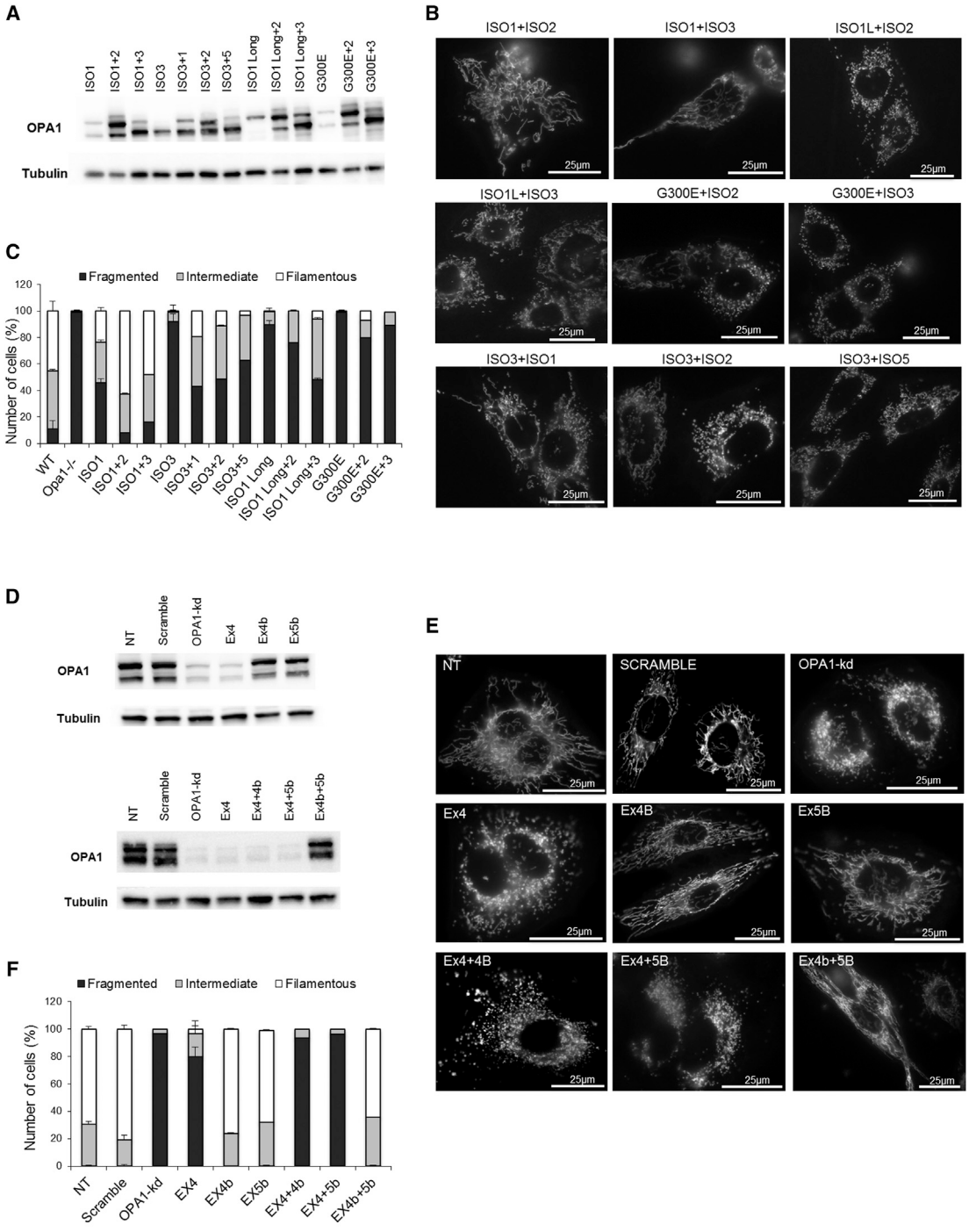

Figure 5. MEFs Co-expressing Two OPA1 Isoforms and Specific OPA1 Isoform Silencing in HeLa Cells

(A) Analysis by western blotting of co-expression of ISO1, ISO2, ISO3, or ISO5 constructs in *Opa1*$^{-/-}$ cells stably expressing ISO1, ISO1 Long, ISO3, or G300E, as indicated. Tubulin was used as a loading control. A representative experiment of three is shown.

(B) Representative images of mitochondrial network of MEFs loaded with Mitotracker Red.

(C) Mitochondrial network was scored as in Figure 1C; 60–80 cells were scored for each cell line. Data are means ± SEM of three independent experiments.

(D) HeLa cells were transfected with siRNA matching the alternatively spliced exons, siEx4, siEx4b and siEx5b, or their combinations (siEx4 + 4b, siRNAEx4 + 5b, and siRNA Ex4b + 5b) with the OPA1-siRNA, or with the scramble siRNA as control, and processed 48 hr after transfection. Western blot of OPA1 expression levels is shown; tubulin was used as a loading control. A representative experiment of three is shown.

(E) Representative images of mitochondrial network of HeLa cells loaded with Mitotracker Red.

(F) Mitochondrial network was scored as in Figure 1C; 50–60 cells were scored for each siRNA. Data are means ± SEM of three independent experiments.

conditions of these studies with our experimental design, opposing the presence of the eight OPA1 isoforms to the single one expressed in our cell model. In rat retinal cells, ischemia-reperfusion (I/R) injury dramatically promoted the accumulation of OPA1 s-forms and cell death, a process that was counteracted by the overexpression of ISO1 Long (Sun et al., 2016). Concordantly, we demonstrate that co-expression of ISO1 Long and the ISO3, generating only s-forms, resulted in a synergistic increase of mitochondrial tubulation in *Opa1*$^{-/-}$ MEFs. Thus, the s-form, in addition to be involved in fusion, works together with the l-form to maintain a filamentous network.

This line of reasoning does not exclude that s-forms may be indirectly involved in fission, as previously proposed (Anand et al., 2014). The minimal fusogenic propensity of s-forms, in fact, may favor fission to prevail.

Our current results additionally establish that a specific combination of l- and s-forms is required for a filamentous network, fitting the theoretical combination of how many short and long forms are generated by the expression of each isoform. In the context of transient co-expression of a second isoform, with overexpression of both isoforms, only a specific balance of l- and s-forms (2long + 2short or 1long + 2short) allows for the complete rescue of mitochondrial network morphology. In the same set of our experiments, unbalancing toward the l-forms was counterproductive, increasing the mitochondrial network fragmentation. Conversely, results from silencing experiments shed light on a second key feature: the need for an adequate amount of OPA1 protein, still with a precise combination of l- and s-forms, to maintain the normal network morphology (2long + 2short or 2long + 4short).

In addition, our results lead to further conclusions as follows: (1) the recovery of altogether mtDNA content, *cristae* organization, and energetic competence was independent of mitochondrial network morphology; (2) reconstitution of *cristae* structure was intimately related to the maintenance of mtDNA copy number; (3) s-forms rescued *cristae* morphology in the absence of l-forms; and (4) s-forms were more efficient than l-forms in restoring the energetic competence.

Indeed, we observed that all isoforms, as well as ISO1 Long, were able to fully recover mtDNA content and nucleoids, even when the mitochondrial network was completely fragmented, in the presence of variable degrees of fusogenic capacity. We also demonstrate that a minimal reconstitution of *cristae* organization was a prerequisite for the rescue of mtDNA copy number and that the degree of recovery of *cristae* morphology paralleled the increase in nucleoids and mtDNA amount.

The severe disorganization of *cristae* structure in *Opa1*$^{-/-}$ MEFs was consistently recovered by the expression of each isoform, but it needed a functional GTPase domain as an absolute requirement. Interestingly, we found that the s-form alone could rescue *cristae* morphology in the absence of the l-form, although a complex mixture of l- and s-forms was assumed to be required for maintaining the integrity of *cristae* junctions (Frezza et al., 2006). However, according to a recent study (Ding et al., 2015), s-forms directly interact with some subunits of the mitochondrial contact site and *cristae* junction organizing system (MICOS) to maintain the integrity of *cristae* junctions, in line with our current results.

The expression of any single isoform completely recovered the functional and structural energetic deficiencies displayed by *Opa1*$^{-/-}$ MEFs, again independently of mitochondrial network morphology. The mechanism underlying the OPA1-driven recovery of energetic efficiency might be related to the interaction of OPA1 with some subunits of complexes I, II, and III (Zanna et al., 2008), likely stabilizing the respirasome and its functions. Remarkably, we found that mitochondrial respiratory competence was not strictly dependent only on mtDNA content and *cristae* organization, but it also required proper proteolytic processing to produce the s-forms. Indeed, ISO1 Long MEFs had only limited efficiency in mitochondrial respiration and presented a reduced amount of assembled supercomplexes, as compared to ISO1 MEFs, suggesting that the l-form alone can only partially rescue bioenergetics, despite having a similar mtDNA amount. Instead, the fully processed s-form alone (e.g., ISO3) was more effective than the uncleavable l-form (ISO1 Long) in rescuing bioenergetics.

Summarizing the OPA1 mitochondrial functions, the structural (*cristae* morphology), genetic (mtDNA amount), and functional (OXPHOS efficiency) features required for mitochondria physiology can be reached by expressing any of the OPA1 isoforms. This is a pre-requisite to fully recover the correct dynamics of mitochondrial network (Figure 6A). The framework for OPA1 that we propose implies that any OPA1 isoform provides an s-form, possibly capable to generate a scaffolding passive structure, on which is wrapped the *cristae* membrane, mandatory for anchoring the mtDNA (Elachouri et al., 2011) and organizing the respirasome, by direct interaction with the respiratory complexes (Zanna et al., 2008). Instead, the l-forms are anchored to the IMM and may be facing the OMM, with an active function in fusion, promoted by the interaction with the mitofusins1/2 (Figure 6B). Then, why do we need both l- and s-forms for an interconnected mitochondrial network? Because, the active l-form (pro-fusion) needs the passive s-form (pro-scaffolding structure) to maintain over time the mitochondria joined into an interconnected network.

In addition, the multiplicity of OPA1 isoforms is required to finely tune and provide flexibility in the execution of mitochondrial dynamics under different cellular conditions. From the evolutionary point of view, this plethora of OPA1 isoforms in metazoans may be related to strictly and timely adapting mitochondrial dynamics to the numerous metabolic conditions and stresses that may jeopardize mitochondrial homeostasis in highly specialized tissues.

Finally, our overall objective, the precise understanding of the role played by each OPA1 isoform or by their combinations, is crucial for the translational implications in human pathology. In particular, OPA1 haploinsufficiency leading to DOA may be amenable to gene therapy approaches, aimed at complementing the *OPA1* null allele. The eye is currently one of the best targets for gene therapy, as indicated by the existing trials on Leber's congenital amaurosis (trial NCT00999609) and Leber's hereditary optic neuropathy (trials NCT02652767 and NCT02652780). Our current results are instrumental to rapidly translating the gene therapy approach for DOA into preclinical experimentation. To this end, we will investigate the pattern of OPA1 isoforms in human retinal ganglion cells, in particular their

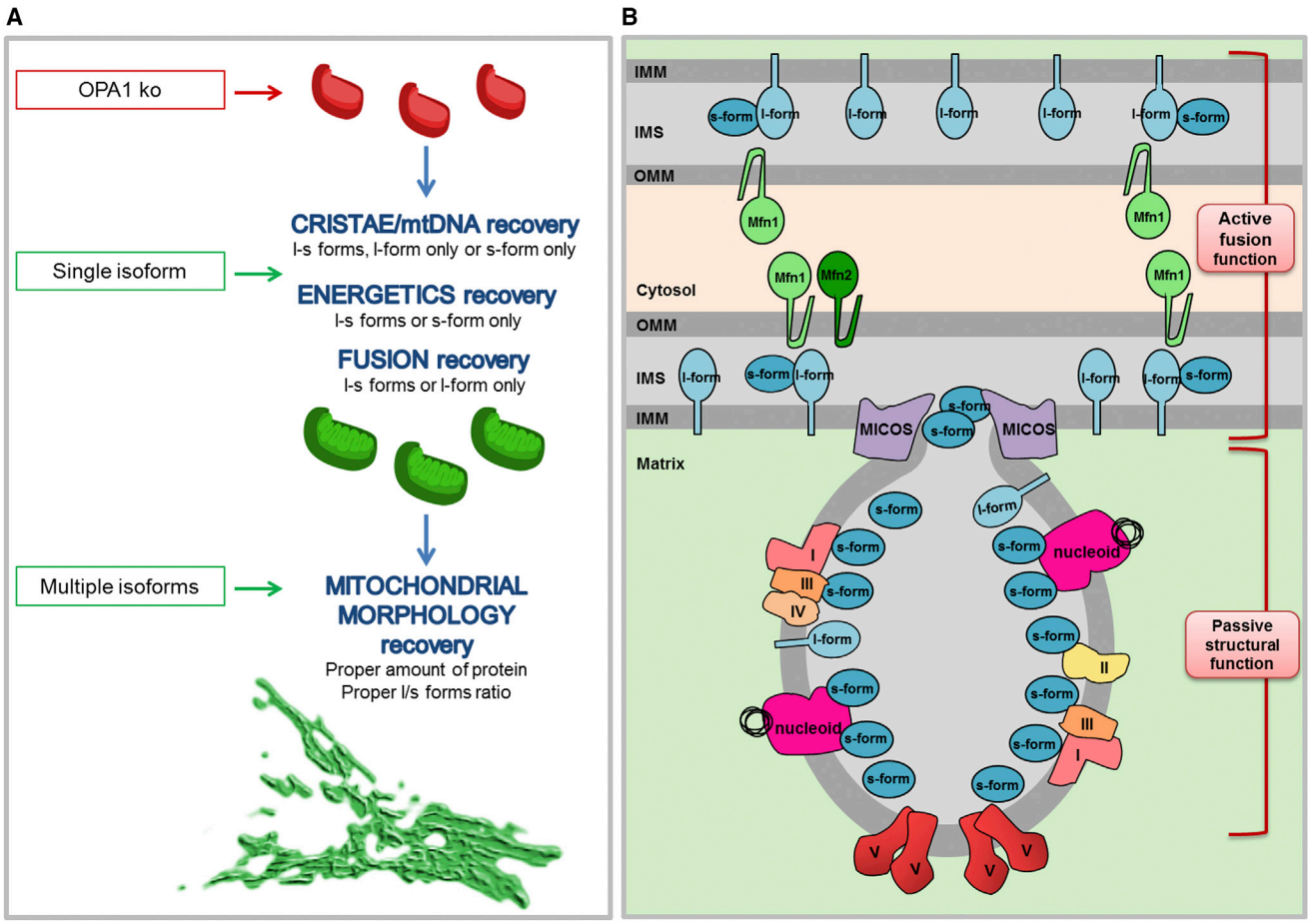

Figure 6. Schematic Representation of the Hierarchic Features Rescued by OPA1 and a Model of Long and Short Form Functions

(A) The expression of one isoform generating long form only (i.e., ISO1 Long) or short form only (i.e., ISO3) is sufficient to induce the total recovery of mtDNA content and *cristae* organization. The expression of any of the eight OPA1 isoforms, including a fully cleaved isoform, is sufficient to promote the complete rescue of the energetic competence, whereas the presence of a long form (i.e., ISO1 Long) is necessary to rescue the mitochondrial fusion. To reach the complete rescue of mitochondrial morphology, at least two isoforms are required with the correct abundance and balance between l- and s-forms.

(B) Any OPA1 isoform provides an s-form that possibly generates a scaffolding passive structure, on which is wrapped the *cristae* membrane, mandatory for anchoring the mtDNA and organizing the respirasome. Instead, the l-forms are anchored to the IMM, mainly facing the OMM, with an active function in fusion, promoted by the interaction with mitofusins1/2.

amount and combination. In fact, based on the understanding reached by this study, the choice of the optimal isoform to re-express by gene therapy must satisfy the requirements for appropriate OPA1 amount and balance between l- and s-forms, and it needs to be tested in a context of neuronal cells reproducing the pathological condition.

EXPERIMENTAL PROCEDURES

Cells and Culture Conditions

MEFs and HeLa cells were grown in DMEM, containing 25 mM glucose supplemented with 10% fetal bovine serum (FBS; Gibco, Life Technologies), 2 mM L-glutamine, 100 U/mL penicillin, and 100 μg/mL streptomycin, in an incubator with a humidified atmosphere of 5% CO_2 at 37°C. For some experiments, cells were grown in glucose-free DMEM supplemented with 5 mM galactose, 5 mM sodium pyruvate, and 5% FBS (DMEM-galactose) and HBSS (Life Technologies).

Plasmid Construction and Retroviral Transduction

Plasmids expressing the eight human OPA1 isoforms, the isoform 1 Long, and bearing the G300E mutation were previously described (Song et al., 2007; Ban et al., 2010). Open reading frames corresponding to residues 1–95 of mouse AIF and 230–960 of human ISO1 were cloned by PCR into the pMSCV-puro vector (see list of primer sequences in the Supplemental Experimental Procedures). Retrovirus production and infection were performed as described previously (Chen et al., 2003). Plasmid (6 μg/experiment) transfection of MEFs was performed with Lipofectamine 3000 (Life Technologies), following the manufacturer's instructions.

Cell Viability Measurement

MEFs (2×10^4/well) were seeded in 24-well plates and incubated with DMEM or DMEM-galactose. Cell viability was determined by using the sulforhodamine B (SRB) assay (Porcelli et al., 2008).

ATP Synthesis Assay

The mitochondrial ATP synthesis was measured in digitonin-permeabilized cells as previously described (Zanna et al., 2008), with minor modifications

by using the luciferin/luciferase assay. Briefly, cells (10^6/mL) were incubated in 150 mM KCl, 25 mM Tris-HCl, 2 mM EDTA, 0.1% BSA, 10 mM potassium-phosphate, 0.1 mM $MgCl_2$ (pH 7.4), 0.1 mM P^1,P^5-di(adenosine-5) pentaphosphate (AP_5A, inhibitor of adenylate kinase), with 50 μg/mL digitonin. Aliquots of 3 × 10^5 cells were incubated in the same buffer in the presence of substrates of CI (1 mM malate plus 1 mM pyruvate) or CII (4 mM succinate plus 5 μM rotenone) or GPD (20 mM glycerol-3-phosphate plus 5 μM rotenone and 5 mM malonate) or CIII (50 μM DBH_2 plus 5 μM rotenone and 5 mM malonate). After the addition of 80 μM ADP, chemiluminescence was determined as a function of time with a luminometer (BioOrbit). The chemiluminescence signal was calibrated with 10 μM ATP, as internal standard, after the addition of 5 μM oligomycin. The rates of ATP synthesis were normalized to protein contents (Bradford, 1976) and citrate synthase (CS) activity (Trounce et al., 1996).

Determination of OCR

The OCR was measured in a Seahorse Biosciences Extracellular Flux Analyzer (model XF96). Oxygen levels were measured over 5-min periods, in basal condition and after the injection of 5 μM oligomycin, 5 μM carbonyl cyanide m-chlorophenyl hydrazone (CCCP), and 5 μM antimycin A. The OCR values (pmol O_2/min) were normalized for protein content of each well, determined by the SRB assay.

H_2O_2 Production and Carbonylated Protein Analysis

H_2O_2 was measured using the ROS-Glo H_2O_2 Assay (Promega), according to the manufacturer's protocol. Evaluation of carbonylated proteins was performed as previously described (Giordano et al., 2015).

Mitochondrial Network Morphology by Confocal Microscopy

MEFs were fixed with pre-warmed formalin for 15 min, and permeabilized with ice-cold acetone for 10 min at −20°C. Mitochondria were labeled by incubating cells in PBS containing 5% FBS and 0.1% Triton X-100 for 2 hr with the anti-Tom-20 antibody and 1 hr with Alexa-Fluor546-conjugated secondary antibody. Images were captured by using a confocal microscope (Zeiss LSM 710) with a 63× oil objective. Cells were scored into three categories as follows: filamentous, intermediate, and fragmented mitochondria; 100 cells were scored for each cell line by blind test. Data are means ± SEM of three independent experiments.

Mitochondrial Network Morphology by Fluorescence Microscopy

MEFs or HeLa cells were stained with 10 nM Mitotracker Red (Life Technologies) for 30 min at 37°C. Live-cell fluorescence images were captured with an inverted Nikon Eclipse Ti-U epifluorescence microscope, using a 63×/1.4-numerical aperture (NA) oil objective, acquired and analyzed by Metamorph software (Universal Imaging). Cells were scored into three categories as follows: filamentous, intermediate, and fragmented mitochondria; 50 cells were scored for each cell line by blind test. Data are means ± SEM of three independent experiments.

Quantification of Mitochondrial Fusion

Cells were transfected with 0.8 μg mt-PAGFP (Abrams et al., 2015) and 0.2 μg mitochondrial P1TS RFP (Oca-Cossio et al., 2003), herein named mt-RFP. Images were captured with an A1 confocal microscope (Nikon Instruments) using a 60×/1.4-NA oil objective. After acquisition of the pre-activated image, regions of interest were selected and activated with the 405-nm laser. The post-activation image was immediately acquired using the 488-nm and 561-nm lasers (1 min), and subsequent images were taken at 30, 60, and 90 min. The z stack images used a step size of 0.7 μm. Mitochondrial fusion was analyzed as previously described (Zanna et al., 2008), with minor modifications. The ratios between the volume of mitochondria with activated mt-PAGFP (by thresholding the image stacks of mt-PAGFP) and the total volume of mitochondria (by thresholding the image stacks of mt-RFP) at each time point were used to quantify mitochondrial fusion. Image analysis was performed using the NIS-Elements software (Nikon Instruments); 20 cells for each cell line were analyzed. For statistical analysis, the Dunnett's multiple comparison test was used.

Transmission Electron Microscopy

Ultrastructural analysis of mitochondria in different MEF cell lines was performed as previously described (Song et al., 2009). Images and the relative quantification refer to focal planes of mitochondria.

mtDNA Content

Isolation and quantification of mtDNA copy number relative to nuclear DNA (nDNA) were performed as previously described (Chen et al., 2010). Quantification of relative copy number was carried out by analysis of the difference in threshold amplification between mtDNA and nuclear DNA (delta delta C[t] method). For statistical analysis, the Dunnett's multiple comparison test was used.

Quantification of Nucleoids

Immunostaining of mitochondrial nucleoid was performed as described in Elachouri et al. (2011). Images were captured with an A1 confocal microscope (Nikon Instruments) using a 60×/1.4-NA oil objective, and nucleoids were quantified using the NIS-Elements software (Nikon Instruments). For statistical analysis, the Dunnett's multiple comparison test was used.

Western Blotting

Cell lysates and crude mitochondria were prepared as previously described (Zanna et al., 2008). Aliquots were separated by 8% SDS-PAGE and transferred onto nitrocellulose membranes (Bio-Rad). The membranes were incubated overnight at 4°C with the primary antibodies, then visualized using horseradish peroxidase-conjugated secondary antibodies. The chemiluminescence signals were revealed using an enhanced chemiluminescence (ECL) western blotting kit and measured with Gel Logic 1500 Imaging System, Biosense.

Analysis of Respiratory Supercomplexes and Complex V

Mitoplasts were isolated from 10^6 cells/mL using 50 μg/mL digitonin, suspended in PBS, and protein content was determined. After centrifugation, the pellet was suspended (5 mg protein/mL) in 150 mM K-acetate, 30 mM HEPES (pH 7.4), 10% glycerol, 1 mM PMSF, and 1% (w/v) digitonin and incubated on ice for 30 min. Samples were centrifuged and aliquots of supernatant were separated on 3%–12% gradient gel (Calvaruso et al., 2012). Gels were analyzed for CI IGA (Porcelli et al., 2009) and western blotting with antibodies against representative subunits of each complex.

RNAi

Transfections of HeLa cells were performed with Lipofectamine RNAiMAX (Life Technologies), following the manufacturer's instructions. Final concentration of siRNA in culture medium was 10 nM. The siRNA (Life Technologies) exon-specific sequences are as follows: OPA1-kd (5-GUUAUCAGUCU GAGCCAGGTT-3); Ex4 OPA (5-GAUUGUUGAAAGCCUUAGCTT-3); Ex4b OPA1 (5-GUCAUAGGAGCUUCUGACCTT-3); and Ex5b OPA1 (5-GAGGAA GCGCGCAGAGCCGTT-3).

Reagents

Antibodies were as follows: Actin (Millipore); Drp1, Mfn1, and Mfn2 (Abnova); NDUFA9 CI, SDHA CII, Core2 CIII, and α and β subunits of CV (MitoSciences); OPA1 and TIM23 (BD Biosciences); TOM20 (Santa Cruz Biotechnology); and β-tubulin (Sigma-Aldrich). Horseradish peroxidase-conjugated secondary antibodies were from Jackson ImmunoResearch Laboratories or Alexafluor, and the ECL western blotting kit was from Amersham Bioscience. All the other reagents were from Sigma-Aldrich.

Statistical Analysis

All numerical data are expressed as mean ± SD or SEM, as indicated. Student's unpaired two-tailed t test was used for statistical analysis, unless otherwise indicated. Differences were considered statistically significant for $p < 0.05$.

SUPPLEMENTAL INFORMATION

Supplemental Information includes Supplemental Experimental Procedures and five figures and can be found with this article online at http://dx.doi.org/10.1016/j.celrep.2017.05.073.

AUTHOR CONTRIBUTIONS

Conceptualization, V.D.D., M.R., and C.Z.; Methodology, V.D.D.; Investigation, V.D.D., P.M., S.V., M.F., A.M., L.C., J.M.M., M.C., and C.Z.; Resources, D.C. and G.L.; Writing – Original Draft, V.D.D. and C.Z.; Writing – Review & Editing, V.D.D., P.M., E.B., G.L., V.C., D.C., M.R., and C.Z.; Visualization, V.D.D. and C.Z.; Funding Acquisition, D.C., V.C., M.R., and C.Z.; Supervision, V.C., D.C., M.R., and C.Z.; Project Administration, C.Z.

ACKNOWLEDGMENTS

This research was supported by grants from Ministero della Istruzione Università e Ricerca, MIUR (FIR2013 grant J38C13001770001 to C.Z. and PRIN grant 20107Z8XBW to M.R.), the NIH (grant GM110039 to D.C.), and E-Rare project 2009-ERMION to V.C., M.R., and G.L. V.D.D. was the recipient of a Marco Polo fellowship, University of Bologna.

Received: October 17, 2016
Revised: April 15, 2017
Accepted: May 23, 2017
Published: June 20, 2017

REFERENCES

Abrams, A.J., Hufnagel, R.B., Rebelo, A., Zanna, C., Patel, N., Gonzalez, M.A., Campeanu, I.J., Griffin, L.B., Groenewald, S., Strickland, A.V., et al. (2015). Mutations in SLC25A46, encoding a UGO1-like protein, cause an optic atrophy spectrum disorder. Nat. Genet. *47*, 926–932.

Alexander, C., Votruba, M., Pesch, U.E., Thiselton, D.L., Mayer, S., Moore, A., Rodriguez, M., Kellner, U., Leo-Kottler, B., Auburger, G., et al. (2000). OPA1, encoding a dynamin-related GTPase, is mutated in autosomal dominant optic atrophy linked to chromosome 3q28. Nat. Genet. *26*, 211–215.

Anand, R., Wai, T., Baker, M.J., Kladt, N., Schauss, A.C., Rugarli, E., and Langer, T. (2014). The i-AAA protease YME1L and OMA1 cleave OPA1 to balance mitochondrial fusion and fission. J. Cell Biol. *204*, 919–929.

Ban, T., Heymann, J.A., Song, Z., Hinshaw, J.E., and Chan, D.C. (2010). OPA1 disease alleles causing dominant optic atrophy have defects in cardiolipin-stimulated GTP hydrolysis and membrane tubulation. Hum. Mol. Genet. *19*, 2113–2122.

Belenguer, P., and Pellegrini, L. (2013). The dynamin GTPase OPA1: more than mitochondria? Biochim. Biophys. Acta *1833*, 176–183.

Bradford, M.M. (1976). A rapid and sensitive method for the quantitation of microgram quantities of protein utilizing the principle of protein-dye binding. Anal. Biochem. *72*, 248–254.

Calvaruso, M.A., Willems, P., van den Brand, M., Valsecchi, F., Kruse, S., Palmiter, R., Smeitink, J., and Nijtmans, L. (2012). Mitochondrial complex III stabilizes complex I in the absence of NDUFS4 to provide partial activity. Hum. Mol. Genet. *21*, 115–120.

Chen, H., Detmer, S.A., Ewald, A.J., Griffin, E.E., Fraser, S.E., and Chan, D.C. (2003). Mitofusins Mfn1 and Mfn2 coordinately regulate mitochondrial fusion and are essential for embryonic development. J. Cell Biol. *160*, 189–200.

Chen, H., Vermulst, M., Wang, Y.E., Chomyn, A., Prolla, T.A., McCaffery, J.M., and Chan, D.C. (2010). Mitochondrial fusion is required for mtDNA stability in skeletal muscle and tolerance of mtDNA mutations. Cell *141*, 280–289.

Cipolat, S., Martins de Brito, O., Dal Zilio, B., and Scorrano, L. (2004). OPA1 requires mitofusin 1 to promote mitochondrial fusion. Proc. Natl. Acad. Sci. USA *101*, 15927–15932.

Cogliati, S., Frezza, C., Soriano, M.E., Varanita, T., Quintana-Cabrera, R., Corrado, M., Cipolat, S., Costa, V., Casarin, A., Gomes, L.C., et al. (2013). Mitochondrial cristae shape determines respiratory chain supercomplexes assembly and respiratory efficiency. Cell *155*, 160–171.

Delettre, C., Lenaers, G., Griffoin, J.M., Gigarel, N., Lorenzo, C., Belenguer, P., Pelloquin, L., Grosgeorge, J., Turc-Carel, C., Perret, E., et al. (2000). Nuclear gene OPA1, encoding a mitochondrial dynamin-related protein, is mutated in dominant optic atrophy. Nat. Genet. *26*, 207–210.

DeVay, R.M., Dominguez-Ramirez, L., Lackner, L.L., Hoppins, S., Stahlberg, H., and Nunnari, J. (2009). Coassembly of Mgm1 isoforms requires cardiolipin and mediates mitochondrial inner membrane fusion. J. Cell Biol. *186*, 793–803.

Ding, C., Wu, Z., Huang, L., Wang, Y., Xue, J., Chen, S., Deng, Z., Wang, L., Song, Z., and Chen, S. (2015). Mitofilin and CHCHD6 physically interact with Sam50 to sustain cristae structure. Sci. Rep. *5*, 16064.

Elachouri, G., Vidoni, S., Zanna, C., Pattyn, A., Boukhaddaoui, H., Gaget, K., Yu-Wai-Man, P., Gasparre, G., Sarzi, E., Delettre, C., et al. (2011). OPA1 links human mitochondrial genome maintenance to mtDNA replication and distribution. Genome Res. *21*, 12–20.

Frezza, C., Cipolat, S., Martins de Brito, O., Micaroni, M., Beznoussenko, G.V., Rudka, T., Bartoli, D., Polishuck, R.S., Danial, N.N., De Strooper, B., and Scorrano, L. (2006). OPA1 controls apoptotic cristae remodeling independently from mitochondrial fusion. Cell *126*, 177–189.

Giordano, L., Deceglie, S., d'Adamo, P., Valentino, M.L., La Morgia, C., Fracasso, F., Roberti, M., Cappellari, M., Petrosillo, G., Ciaravolo, S., et al. (2015). Cigarette toxicity triggers Leber's hereditary optic neuropathy by affecting mtDNA copy number, oxidative phosphorylation and ROS detoxification pathways. Cell Death Dis. *6*, e2021.

Gomes, L.C., Di Benedetto, G., and Scorrano, L. (2011). Essential amino acids and glutamine regulate induction of mitochondrial elongation during autophagy. Cell Cycle *10*, 2635–2639.

Ishihara, N., Fujita, Y., Oka, T., and Mihara, K. (2006). Regulation of mitochondrial morphology through proteolytic cleavage of OPA1. EMBO J. *25*, 2966–2977.

Lenaers, G., Hamel, C., Delettre, C., Amati-Bonneau, P., Procaccio, V., Bonneau, D., Reynier, P., and Milea, D. (2012). Dominant optic atrophy. Orphanet J. Rare Dis. *7*, 46.

MacVicar, T., and Langer, T. (2016). OPA1 processing in cell death and disease - the long and short of it. J. Cell Sci. *129*, 2297–2306.

Mishra, P., Carelli, V., Manfredi, G., and Chan, D.C. (2014). Proteolytic cleavage of Opa1 stimulates mitochondrial inner membrane fusion and couples fusion to oxidative phosphorylation. Cell Metab. *19*, 630–641.

Oca-Cossio, J., Kenyon, L., Hao, H., and Moraes, C.T. (2003). Limitations of allotopic expression of mitochondrial genes in mammalian cells. Genetics *165*, 707–720.

Olichon, A., Emorine, L.J., Descoins, E., Pelloquin, L., Brichese, L., Gas, N., Guillou, E., Delettre, C., Valette, A., Hamel, C.P., et al. (2002). The human dynamin-related protein OPA1 is anchored to the mitochondrial inner membrane facing the inter-membrane space. FEBS Lett. *523*, 171–176.

Olichon, A., Baricault, L., Gas, N., Guillou, E., Valette, A., Belenguer, P., and Lenaers, G. (2003). Loss of OPA1 perturbates the mitochondrial inner membrane structure and integrity, leading to cytochrome c release and apoptosis. J. Biol. Chem. *278*, 7743–7746.

Olichon, A., Elachouri, G., Baricault, L., Delettre, C., Belenguer, P., and Lenaers, G. (2007a). OPA1 alternate splicing uncouples an evolutionary conserved function in mitochondrial fusion from a vertebrate restricted function in apoptosis. Cell Death Differ. *14*, 682–692.

Olichon, A., Landes, T., Arnauné-Pelloquin, L., Emorine, L.J., Mils, V., Guichet, A., Delettre, C., Hamel, C., Amati-Bonneau, P., Bonneau, D., et al. (2007b). Effects of OPA1 mutations on mitochondrial morphology and apoptosis: relevance to ADOA pathogenesis. J. Cell. Physiol. *211*, 423–430.

Patten, D.A., Wong, J., Khacho, M., Soubannier, V., Mailloux, R.J., Pilon-Larose, K., MacLaurin, J.G., Park, D.S., McBride, H.M., Trinkle-Mulcahy, L., et al. (2014). OPA1-dependent cristae modulation is essential for cellular adaptation to metabolic demand. EMBO J. *33*, 2676–2691.

Porcelli, A.M., Ghelli, A., Iommarini, L., Mariani, E., Hoque, M., Zanna, C., Gasparre, G., and Rugolo, M. (2008). The antioxidant function of Bcl-2 preserves cytoskeletal stability of cells with defective respiratory complex I. Cell. Mol. Life Sci. *65*, 2943–2951.

Porcelli, A.M., Angelin, A., Ghelli, A., Mariani, E., Martinuzzi, A., Carelli, V., Petronilli, V., Bernardi, P., and Rugolo, M. (2009). Respiratory complex I dysfunction due to mitochondrial DNA mutations shifts the voltage threshold for opening of the permeability transition pore toward resting levels. J. Biol. Chem. *284*, 2045–2052.

Song, Z., Chen, H., Fiket, M., Alexander, C., and Chan, D.C. (2007). OPA1 processing controls mitochondrial fusion and is regulated by mRNA splicing, membrane potential, and Yme1L. J. Cell Biol. *178*, 749–755.

Song, Z., Ghochani, M., McCaffery, J.M., Frey, T.G., and Chan, D.C. (2009). Mitofusins and OPA1 mediate sequential steps in mitochondrial membrane fusion. Mol. Biol. Cell *20*, 3525–3532.

Sun, Y., Xue, W., Song, Z., Huang, K., and Zheng, L. (2016). Restoration of Opa1-long isoform inhibits retinal injury-induced neurodegeneration. J. Mol. Med. (Berl.) *94*, 335–346.

Trounce, I.A., Kim, Y.L., Jun, A.S., and Wallace, D.C. (1996). Assessment of mitochondrial oxidative phosphorylation in patient muscle biopsies, lymphoblasts, and transmitochondrial cell lines. Methods Enzymol. *264*, 484–509.

Varanita, T., Soriano, M.E., Romanello, V., Zaglia, T., Quintana-Cabrera, R., Semenzato, M., Menabò, R., Costa, V., Civiletto, G., Pesce, P., et al. (2015). The OPA1-dependent mitochondrial cristae remodeling pathway controls atrophic, apoptotic, and ischemic tissue damage. Cell Metab. *21*, 834–844.

Vidoni, S., Zanna, C., Rugolo, M., Sarzi, E., and Lenaers, G. (2013). Why mitochondria must fuse to maintain their genome integrity. Antioxid. Redox Signal. *19*, 379–388.

Wai, T., García-Prieto, J., Baker, M.J., Merkwirth, C., Benit, P., Rustin, P., Rupérez, F.J., Barbas, C., Ibañez, B., and Langer, T. (2015). Imbalanced OPA1 processing and mitochondrial fragmentation cause heart failure in mice. Science *350*, aad0116.

Zanna, C., Ghelli, A., Porcelli, A.M., Karbowski, M., Youle, R.J., Schimpf, S., Wissinger, B., Pinti, M., Cossarizza, A., Vidoni, S., et al. (2008). OPA1 mutations associated with dominant optic atrophy impair oxidative phosphorylation and mitochondrial fusion. Brain *131*, 352–367.